**Original Article**

# Microstructural and mechanical properties analysis of extruded Sn–0.7Cu solder alloy ☆

CrossMark

*Abdoul-Aziz Bogno[a], José Eduardo Spinelli[b],\*, Conrado Ramos Moreira Afonso[b], Hani Henein[a]*

[a] *Department of Chemical and Materials Engineering, University of Alberta, Edmonton, Alberta, Canada*
[b] *Department of Materials Engineering (DEMa), Federal University of São Carlos (UFSCar), São Carlos, SP , Brazil*

## ARTICLE INFO

## ABSTRACT

The properties and performance of lead-free solder alloys such as fluidity and wettability are defined by the alloy composition and solidification microstructure. Rapid solidification of metallic alloys is known to result in refined microstructures with reduced microsegregation and improved mechanical properties of the final products as compared to normal castings. The rapidly solidified Sn-based solders by melt spinning were shown to be suitable for soldering with low temperature and short soldering duration. In the present study, rapidly solidified Sn–0.7 wt.%Cu droplets generated by impulse atomization (IA) were achieved as well as directional solidification under transient conditions at lower cooling rate. This paper reports on a comparative study of the rapidly solidified and the directionally solidified samples. Different but complementary characterization techniques were used to fully analyze the solidification microstructures of the samples obtained under the two cooling regimes. These include X-ray diffractometry (XRD) and scanning electron microscopy (SEM). In order to compare the tensile strength and elongation to fracture of the directionally solidified ingot and strip castings with the atomized droplet, compaction and extrusion of the latter were carried out. It was shown that more balanced and superior tensile mechanical properties are available for the hot extruded samples from compacted as-atomized Sn–0.7 wt.%Cu droplets. Further, elongation-to-fracture was 2–3× higher than that obtained for the directionally solidified samples.

## 1. Introduction

Sn–Pb alloys have been replaced by alternative alloys in the last few years due to the imposed restrictions concerning the use of lead (Pb) in industrial processes [1]. Such constraints in the usage of leaded soldering alloys is due to its inherent toxicity to human health and negative impacts on the environment. Nevertheless, the main alternative options such as Sn–Cu, Sn–Zn, Sn–Ag have proved to be inappropriate
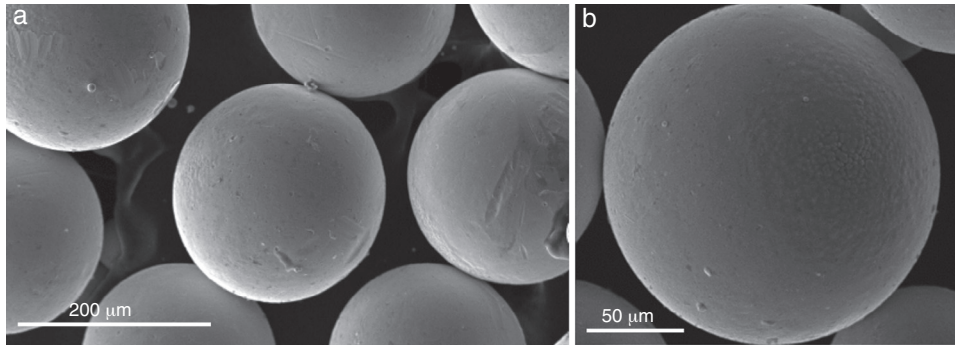
**Fig. 1 – SE-SEM images of the as-atomized Sn–0.7 wt.%Cu alloy droplets of (a) low magnification image, size range 212–250 μm and (b) a higher magnification image, size range 125–150 μm.**
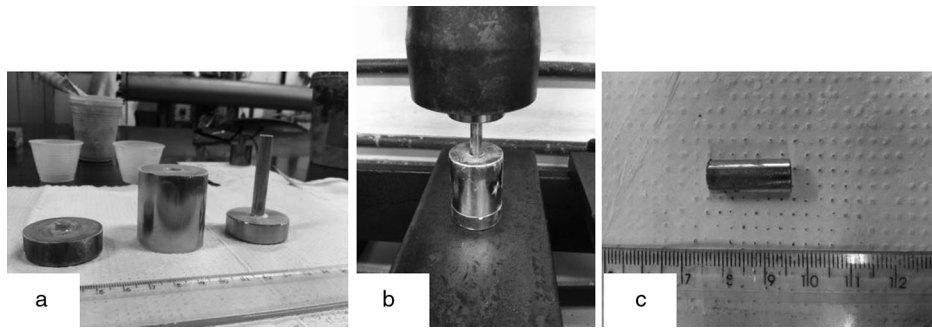


**Fig. 2 – Sequences of the compaction process: (a) parts of the cylindrical cavity to accommodate the atomized Sn–0.7 wt.% Cu droplets; (b) droplets under 2000 kg load during the compaction operation and (c) the resultant cylindrical shape compacted droplets.**

regarding to at least one of the main features stressed as essential to the formation of a solder joint. For example, the intermetallic compounds (IMCs) must be refined and homogeneously distributed within the β-Sn matrix. Thus, for the new solder alloys to become more reliable, associated new routes of processing may be required. As a consequence, some characteristics of the alloys may be modified.

Recent literature [2,3] indicates that one way of improving the properties of the solder is the judicious selection and innovation of the processing techniques. Powder metallurgy is one of the alternatives to produce high performance materials with refined microstructures. Alam and Gupta [4] pointed that higher density and better microstructural properties can be obtained by extruding Sn–Cu samples at high temperature. Moreover, rapid solidification of metallic alloys is known to
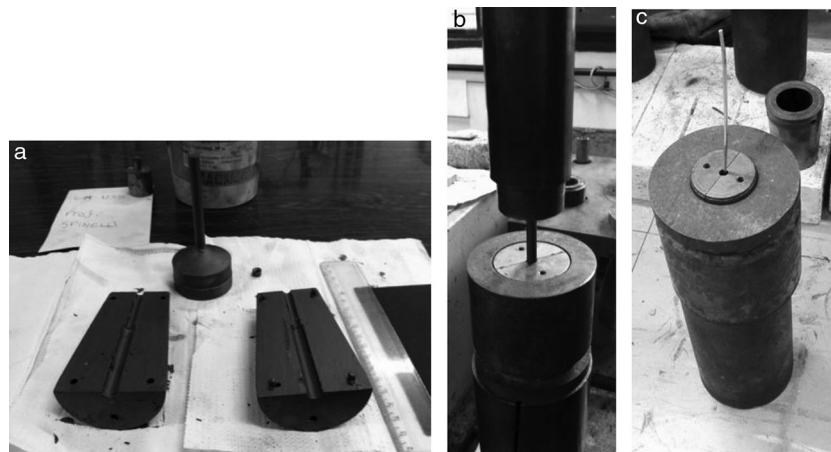


**Fig. 3 – (a) Channeled half-cylinders to extrude the compacted sample through a die located at the narrow bottom end; (b) the mounted assembly placed under a load during extrusion and (c) the extruded rod coming out of the die. Reduction ratio: 10:1; extrusion rate = 5 mm/min.**
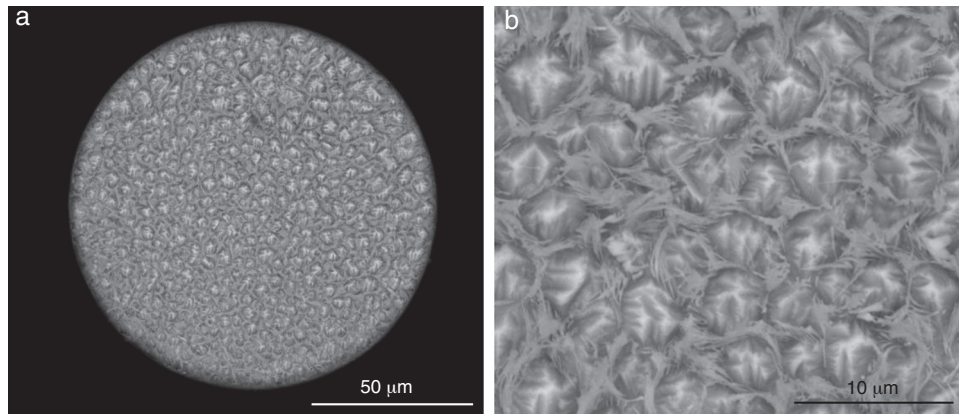
**Fig. 4 – SEM (BSE) images at different magnifications showing microstructures of a Sn–0.7 wt.%Cu alloy droplet with average size of 137.5 μm: (a) global view of the droplet cross-section and (b) a magnified view of the cross-section.**
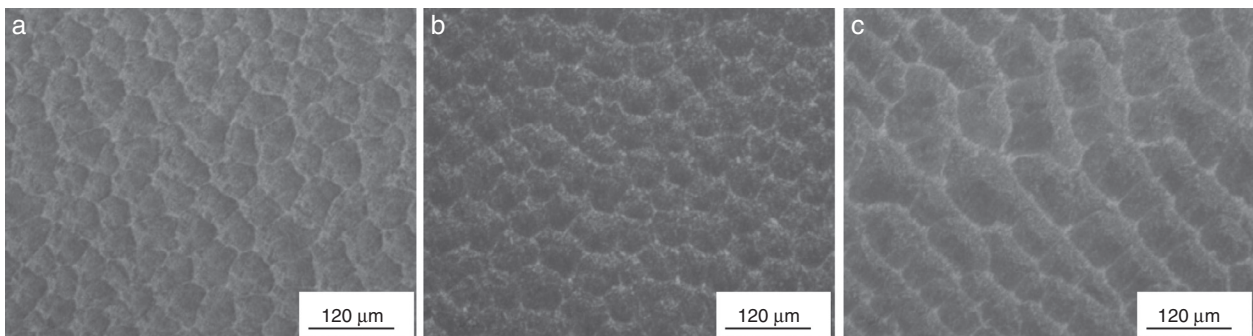


**Fig. 5 – Typical (DS) as-cast microstructures of Sn–0.7 wt.%Cu alloy along the casting length showing the size variation of the eutectic cells as a function of the distance (P) from the metal/mold interface: (a) P = 30 mm, (b) P = 45 mm and (c) P = 80 mm.**

result in refined microstructures with reduced microsegregation and improved mechanical properties of the final products as compared to normal as-cast components [5,6]. Jing and co-authors [7] found that very fine netlike dendritic structure with Zn distributed in a granular form is possible to be obtained in the solder Sn–9Zn alloy foil with a cooling rate in the order of $10^6$ K/s.

Typical cooling rates during reflow procedures for solders in industrial practice remain in the range of 3.0–10.0 K/s [8,9].

Directional solidification (DS) experiments allow the same order of magnitude of cooling rates to be obtained. Final microstructure is a direct consequence of this solidification thermal parameter. DS results have a correspondence with the standard procedures that are used in industry. Much higher cooling rates are experienced by rapidly solidified alloys with uniform chemical composition and lower melting points [5], leading to improved performance of joining due to refined microstructure. Little attention has been given to the
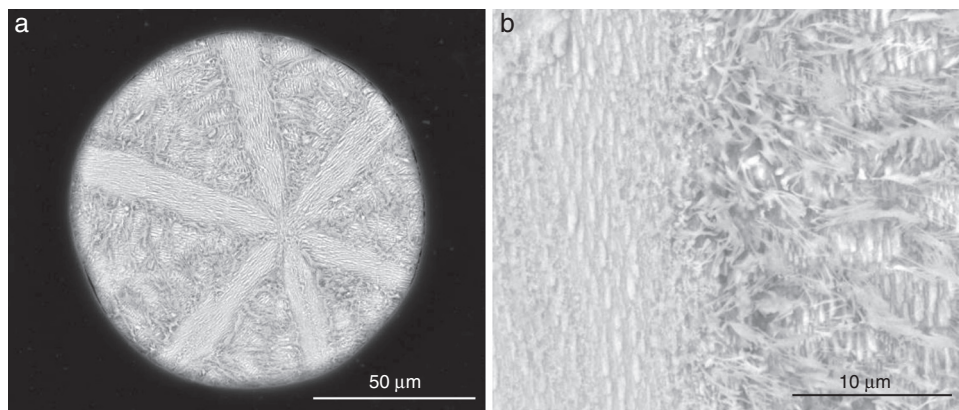


**Fig. 6 – SEM (BSE) images showing (a) the resultant two alternated sizes of eutectics and (b) highly magnified detail of the interface between them.**

| Droplets size range (μm) | Cooling rate (K s$^{-1}$) |
|---|---|
| 125–150 | 123.0 |
| 180–212 | 91.0 |
| 250–300 | 25.0 |

microstructural changes and reliability of the rapidly solidified and extruded Sn–0.7Cu solder alloy.

The rapidly solidified lead-free solders are assumed to propitiate lower melting point, narrower melting interval, better wettability and improved mechanical performance because of the fine, uniform and small segregation microstructure compared with the as-cast lead-free solders [10]. Features such as high melting rate, low soldering temperature and short time are highly desirable concerning real processing conditions, even though rapidly solidified microstructure will be affected during resolidification step within the solder joint.

Jing et al. [7] stated that when rapidly solidified Sn–9Zn alloy was used in soldering, the formation of the massive intermetallic particles at the interface of solder/Cu joints was significantly depressed in comparison with as-cast solder. The microstructure of the joint exhibited finer, more uniform morphology, and the mechanical properties of the solder/Cu joint were improved. Ma and co-authors [11] found that the rapidly solidified Sn–3.5Ag solder may exhibit better wettability. Also, the melting rate is higher for the rapidly solidified Sn–3.5Ag solder.

The main purpose of this work is to study the influence of both atomization and extrusion processes on the final microstructures of the Sn–0.7Cu alloy so that a comparison could be made with directionally solidified specimens. The results corresponding to the two cooling regimes include X-ray diffractometry (XRD), optical microscopy, scanning electron microscopy (SEM) and mechanical tensile tests. An attempt is made in order to correlate the effects of the droplet size and of the extrusion temperature on the microstructural evolution.
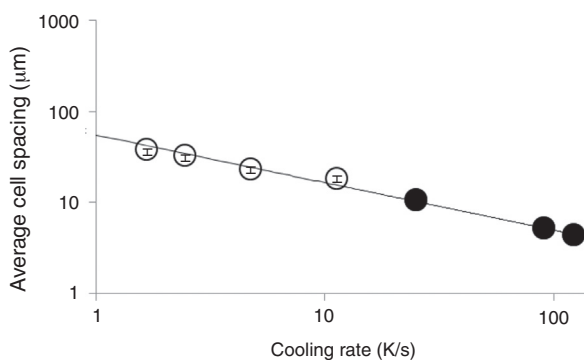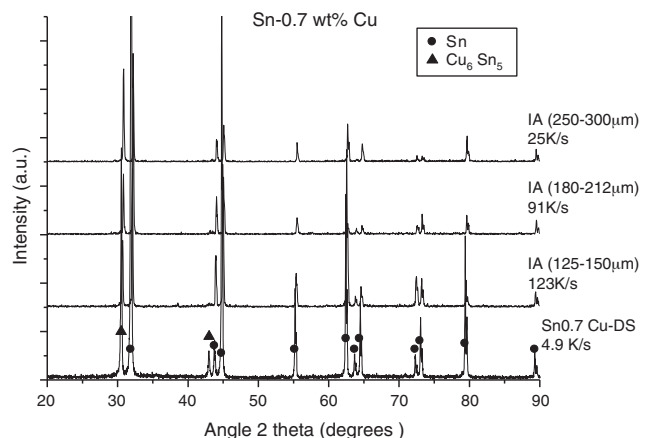
## 2. Experimental procedure

### 2.1. Impulse atomization

Sn–0.7 wt.%Cu alloy (350 g) was prepared at the Advance Materials Processing Laboratory (AMPL) of the University of Alberta. Appropriate weights of commercial Sn shots (99.8% purity) and Cu shots (99.9% purity) were mixed in a clay-graphite crucible and heated to 1200 °C in an induction furnace. The molten alloy was then stabilized for 30 min to allow a complete mixing of the alloy and then cooled to 500 °C before being transformed into spherical droplets that rapidly solidified by impulse atomization (IA) under Argon atmosphere. The droplets were then collected in an oil filled beaker before being washed, dried and sieved into different sizes. Droplet sizes varying from 125 μm to 1000 μm were obtained using nozzle size of 50 μm. Fig. 1 shows an example of the droplets morphology investigated in this work. Three size ranges were examined in the present investigation: 125–150 μm, 180–212 μm and 250–300 μm.

### 2.2. Droplets compaction and extrusion

Single punch compaction of the droplets was performed at room temperature under normal atmosphere using a load of approximately 2000 kg. Sets of droplets with sizes ranging from 125–150 μm and 250–300 μm were introduced in a hollow cylindrical geometry and sandwiched by two T-shape cylinders (Fig. 2a). The assembly was then placed under the 2000 kg load as shown in Fig. 2b. As a result of the compressing of the droplets, a compacted solid (Fig. 2c) was obtained through the cylindrical die. The reduction was estimated to be 60% of the initial volume of the droplets filled cylinder.

After compaction, the samples were extruded at room temperature as well as at 150 °C. The extrusion process described in Fig. 3, consisted in sandwiching a sample in a hollow cylindrical geometry made of two half cylinders with a die placed at the bottom (Fig. 3a). The assembly including a compacted sample of 18 mm in height and 7.6 mm diameter was then put under a load (Fig. 3b). Then, at a rate of 5 mm/min the sample



**Fig. 7 – Average cell spacing variation with cooling rate for the Sn–0.7 wt.%Cu. Open circles refer to the (DS) as-cast samples and solid circles refer to the three size ranges corresponding to the as-atomized droplets under argon.**



**Fig. 8 – XRD patterns of impulse atomized (IA) droplets and of the directionally solidified Sn–0.7 wt.%Cu alloy [14].**
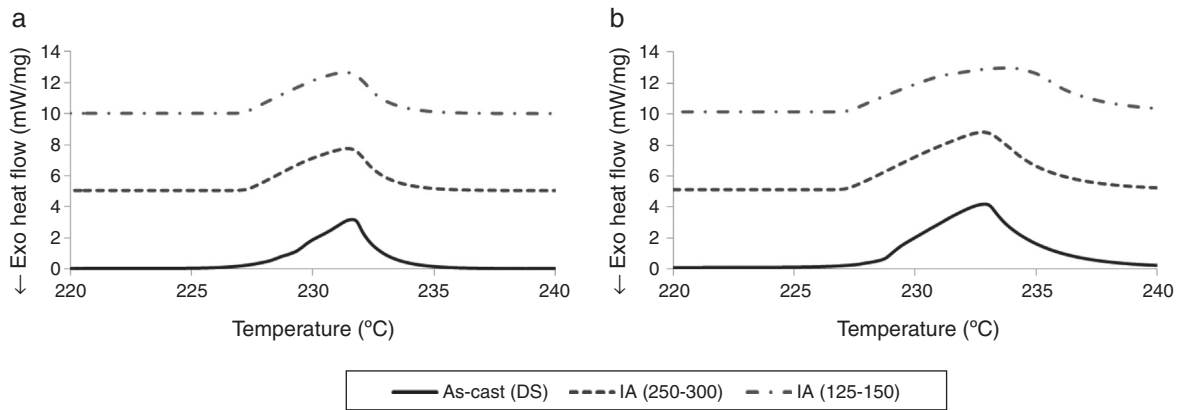
Fig. 9 – DSC heating curves of the three samples heated at (a) 10 K min$^{-1}$; (b) 20 K min$^{-1}$.

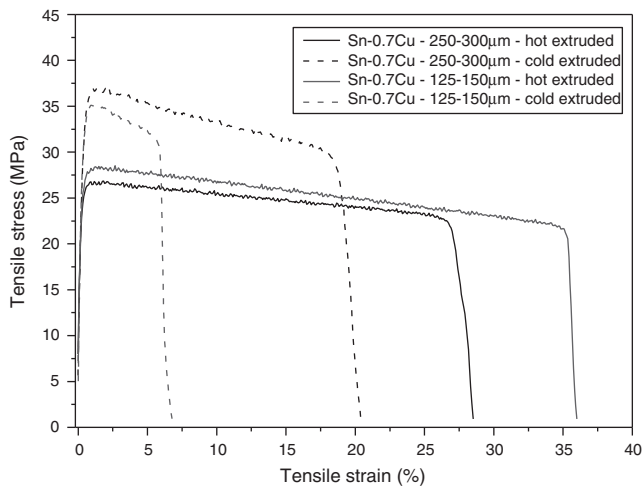| Table 2 – Summary of the results obtained from DSC heating curves of the Sn–0.7 wt.%Cu alloy samples referring to DS and as-atomized conditions. | | | | | | | | |
|---|---|---|---|---|---|---|---|---|
| Heating (K min$^{-1}$) | 125–150 (µm) | | | 250–300 (µm) | | | As-cast (DS) | | |
| | $T_i$ | $T_f$ | $\Delta T$ | $T_i$ | $T_f$ | $\Delta T$ | $T_i$ | $T_f$ | $\Delta T$ |
| 10 | 226 | 233 | 7 | 226 | 233 | 7 | 226 | 233 | 7 |
| 20 | 226 | 238 | 12 | 226 | 238 | 12 | 227 | 238 | 11 |



Fig. 10 – Stress–strain curves of the hot and cold extruded samples (extrusion rate 10:1 and $v$ = 5 mm/min) obtained with the Sn–0.7 wt.%Cu alloy.

was extruded through the dye into a rod of 150 mm long and of 2.5 mm diameter (Fig. 3c), yielding a reduction ratio of 10:1.

### 2.3. Directional solidification

The setup from the Federal University of São Carlos in Brazil (DEMa-UFSCar) was used for directional solidification (DS) casting. It imposes a directional extraction of heat through a water-cooled bottom made of carbon steel (SAE 1020), promoting vertical upward directional solidification. The (DS) casting description is detailed in previous studies [12,13]. The same

Sn–0.7 wt.%Cu melt material used for atomization was directionally solidified.

### 2.4. Microstructure and mechanical characterization of the samples

Selected samples obtained through compaction, extrusion and directional solidification of the Sn–0.7 wt.%Cu alloy were polished and etched (solution of 92% (vol.) CH$_3$OH, 5% (vol.) HNO$_3$ and 3% (vol.) HCl) for metallography. Deep etching procedures were performed up to 3 min, which was enough to partially dissolve the β-Sn matrix. An optical image processing system was used to acquire the images. Furthermore, microstructural characterization was performed using a Field Emission Gun–Scanning Electron Microscope (SEM) Philips (XL30 FEG). Tensile testing on the as-extruded Sn–0.7 wt.%Cu alloy samples was performed according to specifications of ASTM Standard E 8M/04 and tested in a Instron 5500R machine at a strain rate of about $3 \times 10^{-4}$ s$^{-1}$. X-ray diffraction (XRD) patterns were obtained with a 2-theta range from 20° to 90°, Cu-Kα radiation with a wavelength, λ, of 0.15406 nm.

## 3. Results and discussion

### 3.1. Effects of rapid solidification on Sn–0.7 wt.%Cu microstructures

A comparison between the as-atomized droplets and a (DS) as-cast ingot shows that both the atomized and as-cast microstructures present eutectic cells in which the Cu$_6$Sn$_5$ intermetallic compounds (IMCs) can be seen (see Figs. 4 and 5).

The atomized droplets, however, depict two eutectic structures with different morphologies, mean interphase

**Table 3 – Summary of the tensile strength results for the extruded samples.**

| Extruded sample size range (µm) | Extrusion temperature (°C) | Ultimate tensile strength – $\sigma_u$ (MPa) | Elongation to fracture – $\delta$ (%) |
|---|---|---|---|
| 125–150 | 150 | 28.4 | 36.0 |
| 250–300 | | 27.0 | 28.6 |
| 125–150 | Room | 35.1 | 7.0 |
| 250–300 | Temperature | 37.0 | 20.5 |
| DS – as-cast[b] | | 21.0–26.0[a] | 10.5–14.6[a] |

[a] The range of values for the different positions along the DS as-cast samples [16].
[b] The DS as-cast sample was not extruded.

spacing and fibers size (Fig. 6a). It seems that one, a lamellar eutectic structure, develops from a nucleation site and another one a degenerate eutectic (finer $Cu_6Sn_5$ IMC and smaller interphase spacing) as magnified in Fig. 6b. This unusual observation was also reported by Drevet and coworkers [14]. The degenerate morphology is likely due to the Pb impurity (0.017 wt.%) in the commercial feedstock [15].

Eutectic cells spacing variation with cooling rate was analyzed for as-atomized droplets and compared with results obtained for (DS) as-cast samples. Cooling rates corresponding to the investigated droplet sizes have been estimated using the relationship: $\lambda_c = A\dot{T}^{-n}$ established between the cell spacing and the cooling rate ($\dot{T}$) for the (DS) as-cast sample. $A$ and $n$ which are alloy-dependent parameters are found to be 62 and 0.55, respectively [16]. Table 1 gives a
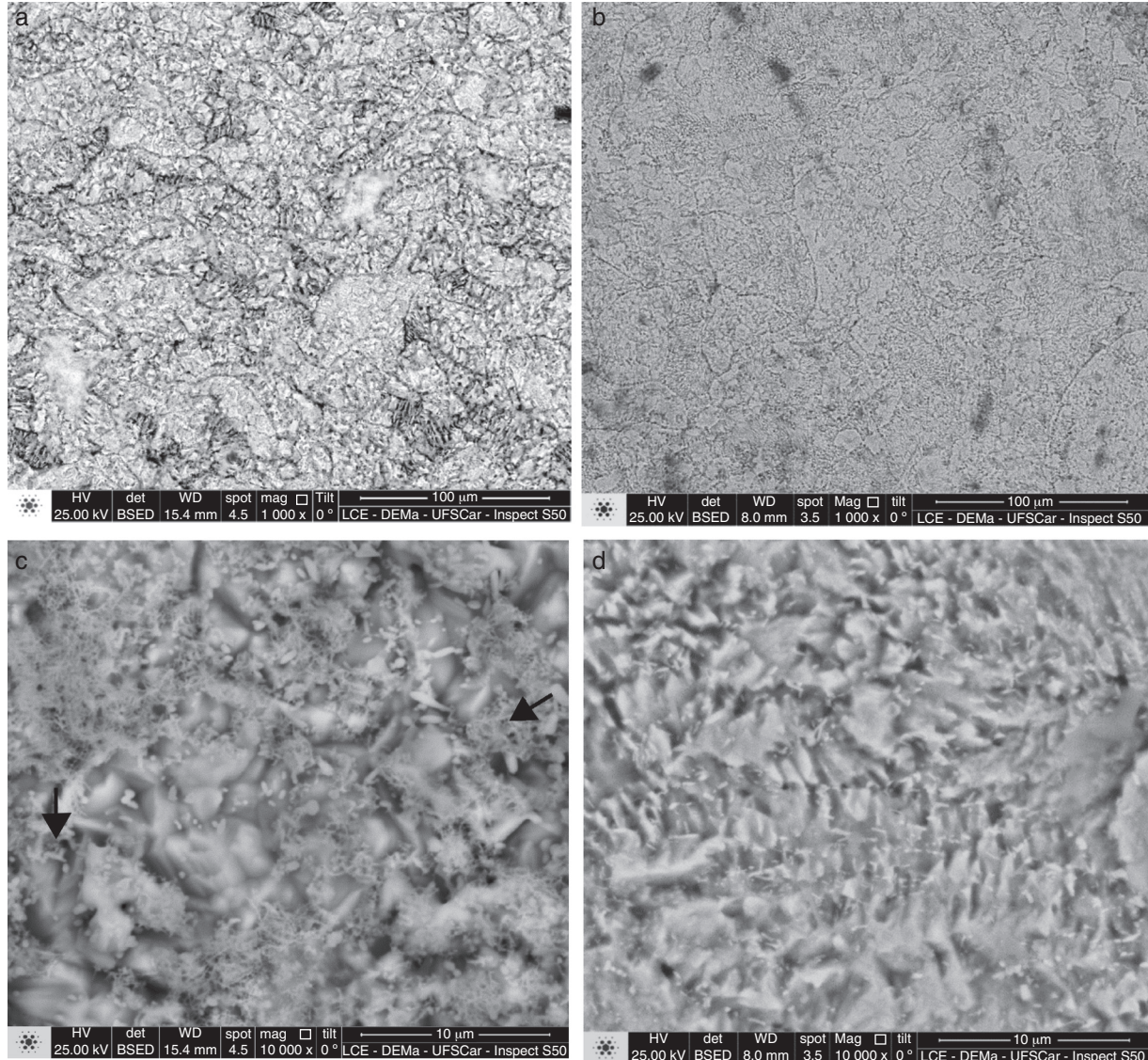


**Fig. 11 – SEM (BSE) microstructures of the Sn–0.7 wt.%Cu alloy droplet with size of 250–300 µm showing (a and c) features concerning hot extruded and (b and d) cold extruded specimens.**
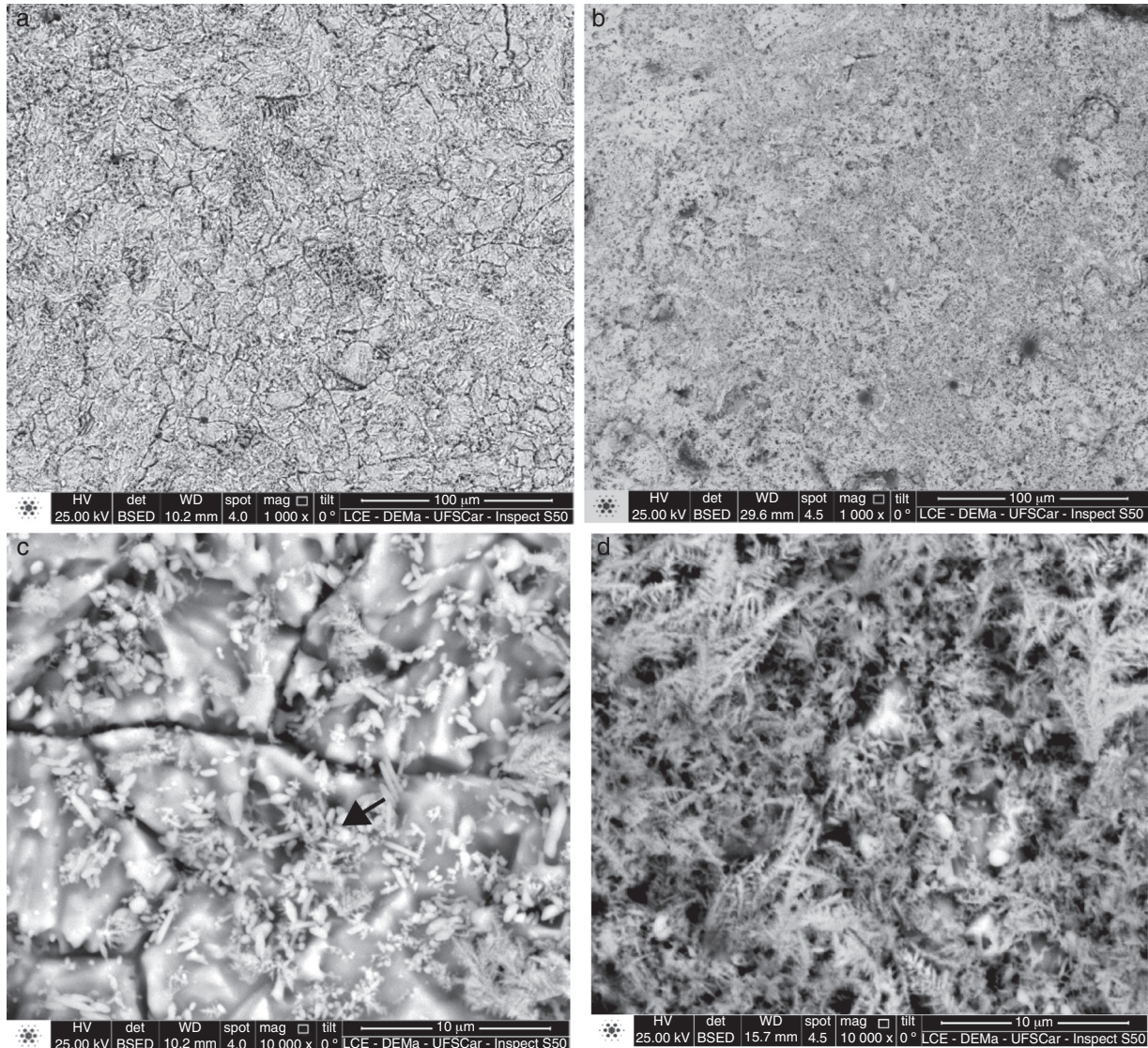
**Fig. 12 – SEM (BSE) microstructures of the Sn–0.7 wt.%Cu alloy droplet with size of 125–150 μm showing (a and c) features concerning hot extruded and (b and d) cold extruded specimens.**

summary of the cooling rates corresponding to the average size of each droplet under investigation. As expected, it was found that the smaller the droplet the higher the cooling rate.

Fig. 7 shows results of eutectic cells spacing variation with cooling rate respectively for three average droplet sizes and the (DS) as-cast sample from different positions along the vertical length of the sample. The results show that cooling rates obtained by impulse atomization are 10 times higher than the ones corresponding to the directionally solidified Sn–0.7 wt.%Cu alloy sample while the cell spacing values are roughly 10 times lower.

### 3.2. Effects of rapid solidification on the formation of phases

Fig. 8 shows the XRD patterns of the as-atomized droplets and of a directionally solidified (DS) as cast sample. Analysis of

the peaks showed evidence of two phases, which are Sn and $Cu_6Sn_5$ in the as atomized samples as well as the (DS) as-cast ones. Therefore, if there is any metastable phases that have formed within the investigated range of cooling rate, it could not be detected by XRD.

### 3.3. Effects of rapid solidification on the melting temperature

Fig. 9 shows DSC heating curves for two different heating rates ($10 \, K \, min^{-1}$ and $20 \, K \, min^{-1}$) of the as-atomized droplets as well as the (DS) as-cast samples. For these DSC experiments, approximately 40 mg of each sample were used in an alumina crucible.

It can be seen from Fig. 9 that the melting starts at the same temperatures (226 °C) for almost all samples at both heating rates excepting in the case of the as-cast (DS) sample at $20 \, K \, min^{-1}$ in which a slightly higher temperature
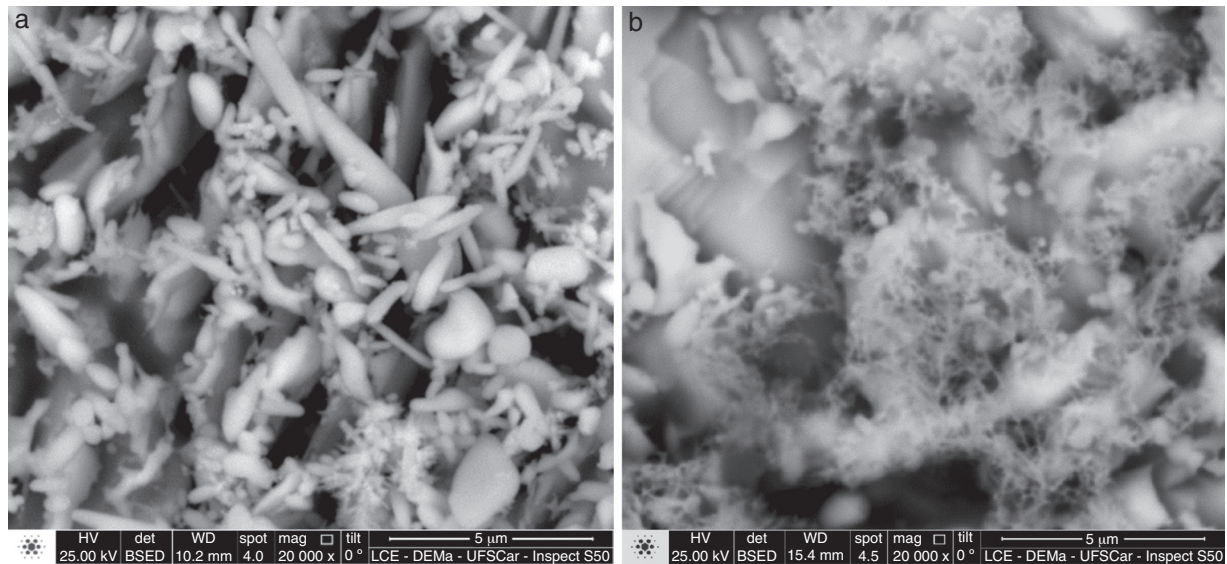
**Fig. 13 – Detailing SEM images (20,000× of magnification) of the Cu$_6$Sn$_5$ IMCs found in the ax-extruded Sn–0.7 wt.%Cu samples: hot extruded droplets with size of (a) 125–150 μm and (b) 250–300 μm.**

is needed in order to start melting. However, the melting interval is larger for the samples heated at a faster rate (20 K min$^{-1}$). And, the melting temperature, corresponding to the peak of the heating curves, was found to be a little higher (~1 °C) for the higher heating rate curves. The measured melting temperatures intervals ($T_i$: start and $T_f$: end) and the melting interval $\Delta T$ are tabulated below for the two different heating rates (Table 2). Thus, the melting interval and the melting point are heating rate dependent due to the thermal resistance of the material and that between the material and the alumina crucible [17]. Further, melting temperature beginning ($T_i$) has been slightly decreased in the case of the as-atomized Sn–0.7 wt.%Cu alloy droplets at 20 K min$^{-1}$.

### 3.4. Effect of rapid solidification on extruded microstructure and tensile properties

Tensile tests were carried out on extruded samples from compacted droplets of different sizes (different cooling rates) at room temperature (so-named cold) as well as heated at 150 °C (so-named hot) and also on the (DS) as-cast sample [16]. A stress–strain curve is plotted for each extruded sample, ultimate tensile stress ($\sigma_u$) as well as elongation to fracture percentage ($\delta$) were determined (Fig. 10). A summary of the results is given in Table 3.

A lower value of around 7% corresponding to the total elongation of the cold extruded sample with 125–150 μm was obtained probably due to the presence of fissures observed all along the examined cross section which anticipated a complete fracture. Such feature has not been observed in the other three tested specimens.

Typical SEM microstructures of the as-extruded Sn–0.7 wt.%Cu alloy are depicted in Figs. 11 and 12 in different magnifications. As it can be seen in Figs 11 and 12, a very low porosity level was obtained. Also, for any examined

droplet size the cold extruded resultant microstructure is characterized by finer grains if compared Figs. 11a, b and 12a, b (low magnification). In general, extrusion procedure has promoted a deep change on the microstructure features since eutectic cells were not identified after such processing. However, microstructures corresponding with the cold extruded samples seem to preserve some characteristics as developed during atomization such as a dendritic morphology of the Cu$_6$Sn$_5$ IMC (see Fig. 12d) and well distributed IMC particles (Fig. 11d) despite being spheroidal in this case. Finer grains seem to be responsible by the higher strength observed for the extruded samples at room temperature. Also, spheroidal (250–300 μm in droplet size) and dendritic (125–150 μm in droplet size) morphologies of the IMCs may contribute to these results concerning mechanical strength.

On the other hand, the extruded samples at 150 °C (Figs. 11c and 12c) are characterized by distinct forms and distributions of the IMCs within the Sn-rich matrix. As pointed by the arrows clustering of rods or very fine alveolar groupings can be observed. Such features corresponding with Sn–0.7 wt.%Cu alloy samples provide a more balanced set of tensile parameters ($\sigma_u$ and $\delta$) as can be seen by the solid lines in Fig. 10. Furthermore, elongation to fracture percent is higher for samples extruded at a temperature of 150 °C as compared to the ones extruded at room temperature.

A previous study on directional solidification of the Sn–0.7 wt.%Cu solder alloy has shown that the average interphase spacing varied from 0.6 to 3.0 μm along the examined casting length [18]. It was measured between the fiber-like Cu$_6$Sn$_5$ particles. As can be seen in Fig. 13 smaller arrangements of this IMC were found on the as-extruded specimens. Essentially due to that the ultimate tensile strengths of the extruded samples from compacted as-atomized Sn–0.7 wt.%Cu droplets are higher than those of the DS as-cast samples. The plastic deformation amount was highly increased in the case of the hot-extruded samples (see Fig. 10).

# 4. Conclusions

Microstructures of IA droplets of different sizes as well as (DS) as-cast Sn–0.7 wt.%Cu samples were analyzed using SEM, DSC and XRD. The following conclusions can be drawn from the present results:

- The eutectic cell sizes are found to be reduced by a factor of 10 when samples are produced by rapid solidification induced IA. The as-atomized samples were successfully compacted at room temperature then extruded at room temperature as well as at 150 °C. The microstructure analysis allowed to estimate the cooling rates experienced by the droplets from 25.0 to 123.0 K/s.
- Cold extruded Sn–0.7 wt.%Cu alloy samples exhibit superior tensile properties as compared to hot extruded ones. However, hot extruded samples permitted a more balanced set of tensile parameters to be obtained, highly increasing elongation-to-fracture values.

## Conflict of interest

The authors declare no conflicts of interest.

## Acknowledgements

R E F E R E N C E S

[1] Wu CML, Yu DQ, Law CMT, Wang L. Properties of lead-free solder alloys with rare earth element additions. Mater Sci Eng R 2004;44:1–44.

[2] Abtew M, Selvaduray G. Lead-free solders in microelectronics. Mater Sci Eng R 2000;27:95–141.

[3] Mahmudi R, Geranmayeh AR, Khanbareh H, Jahangiri N. Design of lead-free candidate alloys for low-temperature soldering applications based on the hypoeutectic Sn–6.5Zn alloy. Mater Des 2009;30:574–80.

[4] Alam ME, Gupta M. Effect of addition of nano-copper and extrusion temperature on the microstructure and mechanical response of tin. J Alloys Compd 2010;490: 110–7.

[5] Kamal M, Gouda ES. Effect of rapid solidification on structure and properties of some lead-free solder alloy. Mater Manuf Process 2006;21:736–40.

[6] Shen J, Liu YC. Microstructure and mechanical properties of lead-free Sn–Cu solder composites prepared by rapid directional solidification. J Mater Sci 2007;18: 1235–8.

[7] Jing Y, Sheng G, Zhao G. Influence of rapid solidification on microstructure, thermodynamic characteristic and the mechanical properties of solder/Cu joints of Sn–9Zn alloy. Mater Des 2013;52:92–7.

[8] Freitas ES, Osorio WR, Spinelli JE, Garcia A. Mechanical and corrosion resistances of a Sn–0.7 wt.%Cu lead-free solder alloy. Microelectron Reliab 2014;54:1392–400.

[9] Spinelli JE, Silva B, Garcia A. Microstructure, phases morphologies and hardness of a Bi–Ag eutectic alloy for high temperature soldering applications. Mater Des 2014;58:482–90.

[10] Ma H, Wang J, Qu L, Zhao N, Kunwar A. A study on the physical properties and interfacial reactions with Cu substrate of rapidly solidified Sn–3.5Ag lead-free solder. J Electron Mater 2013;42:2686–95.

[11] Ma HT, Wang J, Qu L, An LL, Gu LY, Huang ML. The study on the rapidly-solidified Sn–0.7Cu lead-free solders and the interface reactions with Cu substrate. In: International Conference on Electronic Packaging Technology & High Density Packaging. Guilin, Guangxi, China; 2012. p. 361–5.

[12] Rocha OL, Siqueira CA, Garcia A. Cellular/dendritic transition during unsteady-state unidirectional solidification of Sn Pb alloys. Mater Sci Eng A 2003;347:59–69.

[13] Silva AP, Spinelli JE, Mangelinck-Noel N, Garcia A. Microstructural development during transient directional solidification of hypermonotectic Al–Bi alloys. Mater Des 2010;31:4584–91.

[14] Drevet B, Camel D, Dupuy M, Favier JJ. Microstructure of the Sn—$Cu_6Sn_5$ fibrous eutectic and its modification by segregation. Acta Mater 1996;44:4071–84.

[15] Ventura T, Terzia S, Rappaz M, Dahle AK. Effects of solidification kinetics on microstructure formation in binary Sn–Cu solder alloys. Acta Mater 2011;59:1651–8.

[16] Silva BL, Cheung N, Garcia A, Spinelli JE. Thermal parameters, microstructure, and mechanical properties of directionally solidified Sn–0.7 wt.%Cu solder alloys containing 0 ppm to 1000 ppm Ni. J Electron Mater 2013;42:179–91.

[17] Zou C, Gao Y, Yang B, Zhai Q. Melting and solidification properties of the nanoparticles of Sn3.0Ag0.5Cu lead-free solder alloy. Mater Charact 2010;61:474–80.

[18] Moura ITL, Silva CLM, Cheung N, Goulart PR, Garcia A, Spinelli JE. Cellular to dendritic transition during transient solidification of a eutectic Sn 0.7 wt%Cu solder alloy. Mater Chem Phys 2012;132:203–9.